Guan *et al. Soft Sci* 2021;1:16
DOI: 10.20517/ss.2021.19

Soft Science

Review

Open Access

Flexible, high-strength, and porous nano-nano composites based on bacterial cellulose for wearable electronics: a review

Fangyi Guan, Chuan Fei Guo

Department of Materials Science and Engineering, Southern University of Science and Technology, Shenzhen 518055, Guangdong, China.

Correspondence to: Dr. Chuan Fei Guo, Department of Materials Science and Engineering, Southern University of Science and Technology, 1088 Xueyuan Blvd, Shenzhen, Guangdong 518055, China. E-mail: guocf@sustech.edu.cn

How to cite this article: Guan F, Guo CF. Flexible, high-strength, and porous nano-nano composites based on bacterial cellulose for wearable electronics: a review. *Soft Sci* 2021;1:16. https://dx.doi.org/10.20517/ss.2021.19

Received: 20 Nov 2021 **First Decision:** 2 Dec 2021 **Revised:** 16 Dec 2021 **Accepted:** 22 Dec 2021 **Published:** 31 Dec 2021

Academic Editor: Zhifeng Ren **Copy Editor:** Yue-Yue Zhang **Production Editor:** Yue-Yue Zhang

Abstract

Portable flexible electronics based on petroleum-based polymers have stepped onto the stage of modern technology. Increasing environmental problems facilitate emerging technologies based on cellulose because of its abundant sources and the nature of CO_2 consumption and biodegradability. Bacterial cellulose (BC) stands out among all cellulose materials because of its unique features, including the abundant hydrogen bonds, small diameter, three-dimensional nano-networked structures, high purity and crystallinity, and the degree of polymerization. The adequate properties impart BC and its nano-nano composites with superior balance among ductility, strength, and porosity, which are crucial for wearables. The principles of this balance, the fabrication of the nano-nano composites, and the wearable electronic applications based on BC are discussed in detail in this review.

Keywords: bacterial cellulose, strength, porosity, flexibility, nano-nano structure

INTRODUCTION

Tremendous attention has been shifted from conventional solid devices to portable and flexible electronics in recent years due to their huge potential in our future life. Fossil-consuming polymers and their composites are commonly applied in flexible electronics to achieve combined high strength and high

ductility[1]. The modern life is produced because of the use of these petroleum-based polymers, whereas emerging environmental issues, such as global warming and the accumulation of marine microplastics due to their non-biodegradability when the products are discarded, have also been witnessed. The weight of plastic wastes is predicted to surpass that of fish in the oceans by 2050 if the current accumulating speed is maintained[2]. Biomaterials, featured by the virtuous recyclability, are expected to substitute part of the currently used polymers to significantly benefit the sustainability of the environment[3]. Thus far, various natural materials such as chitosan, collagen, terpene, silk, gelatin, and cellulose have been introduced to manufacture flexible electronics[4]. However, the balance among flexibility, strength, and toughness, a crucial property for flexible electronics, is still challenging for most biopolymers[5,6].

Cellulose can be extracted from many sources, including plants, tunicate, fungi, alga, and bacteria. As the most abundant natural polymers, cellulose, united with β-(1→4)-linked d-glucose, is designed from nanoscale to macroscale, resulting in a hierarchical structure[7,8]. Due to the excellent ductility and high strength, cellulose plays a significant role in the manufacturing of flexible electronics by combining with other materials including nanomaterials, or by carbonization. Among all types of cellulose, bacterial cellulose (BC) deserves special attention because of its specific structure and properties, although it shares a chemically equivalent structure with plant cellulose. BC owns a three-dimensional nanofibrous network, resulting in the formation of hydrogel sheets with high surface area and porosity. *Acetobacter xylinum*, the most productive bacteria, polymerizes glucose units into linear β-1,4-glucan chains (protofibrils, about 3 nm width) extracellularly through the bacteria cell wall [Figure 1A][9], assembling together into cellulose ribbons (nanofibrils, 20-100 nm width)[8,10] and then crystallizing into composed ribbons [Figure 1B][11]. Finally, a highly porous web-shaped network is constructed with these ribbons connected through van der Waal forces (vdW forces) [Figure 1C][12,13]. Different from plant fibers that contains only 40%-70% of cellulose due to the presence of lignin, hemicelluloses, and pectin, BC is pure cellulose with up to 90% crystallinity and a degree of polymerization of 8000, leading to high strength up to 300 MPa and low energy consumption dispensing with refining treatments[14,15]. In addition, nanofibers from BC are proven to be finer than those from plant cellulose[16], giving potential for constructing tougher composites. However, BC alone is insufficient to accomplish electrical functions to serve for electronic devices. The porous and H-bond-abundant nature endows BC nanofibers or networks with good housing and anchoring ability; thus, BC is capable of combining nanosized elements to obtain particular composites (called nano-nano composites) for flexible electronics.

The balance among porosity, flexibility, and strength is found in the BC-based nano-nano composites derived from the unique features of BC. In this review, the principles of the property balance, the fabrication methods of the composites, and their wearable or flexible applications are presented.

PRINCIPLE OF CONSTRUCTING BALANCED NANO-NANO STRUCTURE BASED ON BC

One general problem is the contradiction among high flexibility, strength, and porosity for a specific material. For instance, porous foams are often poor in strength; strong polymers or metals usually lack pores; for flexible sheets, their strength and porosity are undesirable. The magic of BC lies in that it well balances all these properties, being flexible, strong, and highly porous.

Six hydroxyl groups in one cellulose molecular unit of BC results in hydrogen bonding sites massively distributed along the free fibril surface. In addition, unlike the isolation between the cellulose nanofibers in plant cell walls due to the presence of lignin and hemicellulose, cellulose bundles and molecules interact with each other more freely without much restriction because of the high purity of cellulose in BC. Both factors bring about high space density of interfacial hydrogen bonding. Moreover, the defect density in BC

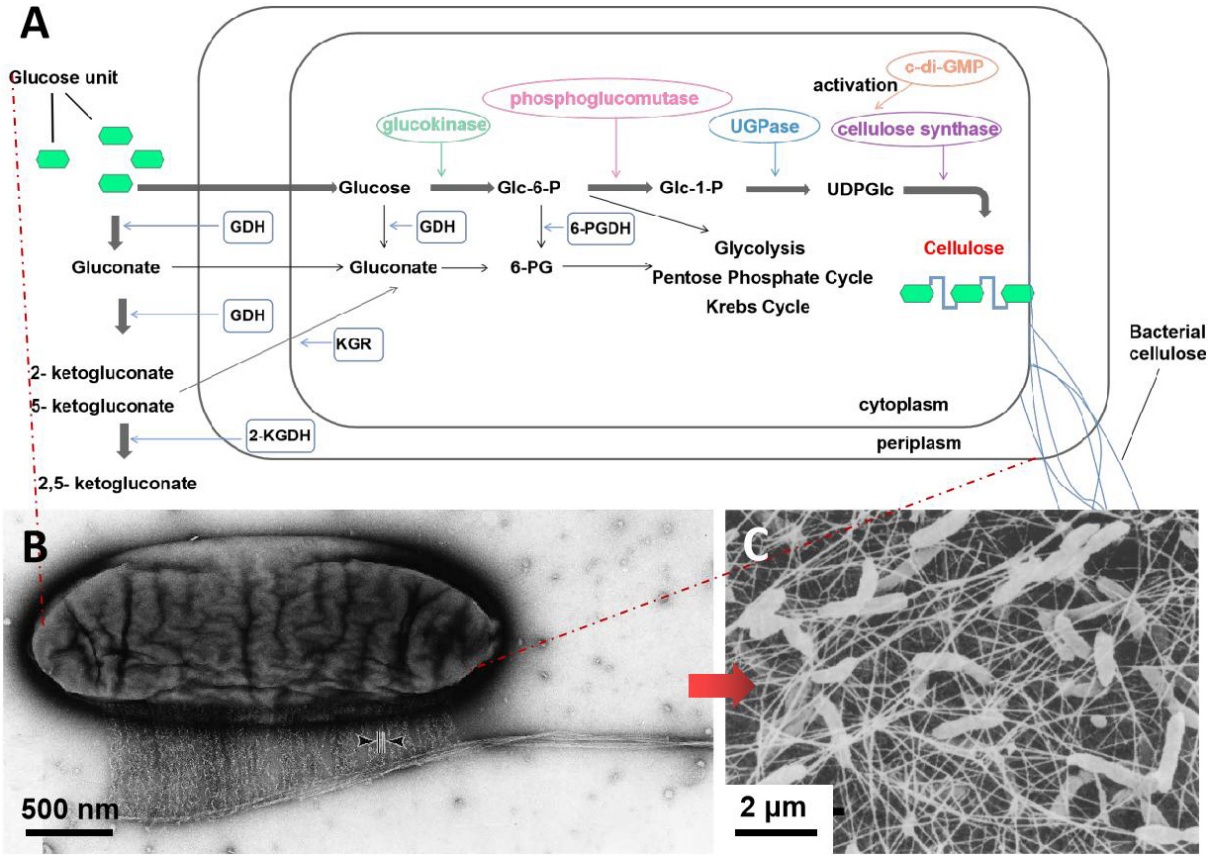

Figure 1. (A) A schematic process of the metabolic pathways of *Acetobacter xylinum* assembling cellulose molecules into nanofibrils. (B) Morphology of *Acetobacter xylinum* producing BC. The arrows refer to the width of cellulose nanofibers. (C) A scanning electron micrograph (SEM) of freeze-dried BC gel. (A) Reproduced with permission[9]. Copyright 2013, Wiley. (B) Reproduced with permission[11]. Copyright 2002, Springer. (C) Reproduced with permission[14]. Copyright 2000, Springer.

is low deriving from the high crystallinity and degree of polymerization (DOP) (≈ 8000) of cellulose molecules[17]. The synergistic effect of high space density of interfacial hydrogen bonding between BC nanofibers and low density of defects gives rise to the high strength of BC.

Furthermore, multiscale mechanical modeling tells that a smaller size of the components results in an enhanced strength of the bulk materials[18]. Because of the nanosize and high crystallinity of the BC bundles, fewer intrinsic natural defects exist compared with other materials or even common plant cellulose. According to fracture mechanics, the strength varies inversely with the square of the fiber diameter[19-22]. Based on the conventional scaling law, "going smaller" brings about higher strength but lower toughness, an immanent problem when designing engineering materials. However, for BC composed of fine nanofibers, the toughness or ductility as an unintentional consequence is high, conforming to the anomalous scaling law - "the smaller, the stronger, and simultaneously the tougher" [Figure 2A-C][18,23]. The tensile strength and toughness of nanopapers made of cellulose nanofibers (CNFs) is obviously superior to that of carbon nanotube (CNT) films despite the same diameter of the nanomaterials (11 nm) (Figure 2, inset image). The improved toughness of CNFs derives from the inter-fiber sliding demonstrated by atomistic simulations [Figure 2D and E][23,24]. At the (110)-(110) interface [Figure 2D], when imposed to continuous shearing, the cellulose chains change from aligned configurations (Location 1) to misaligned configurations (Locations 2), and then they become realigned (Locations 3), as shown in Figure 2E[25]. In the three stages, the hydrogen bond (H-bond) number is the highest at the beginning (Locations 1) and changes dynamically as the

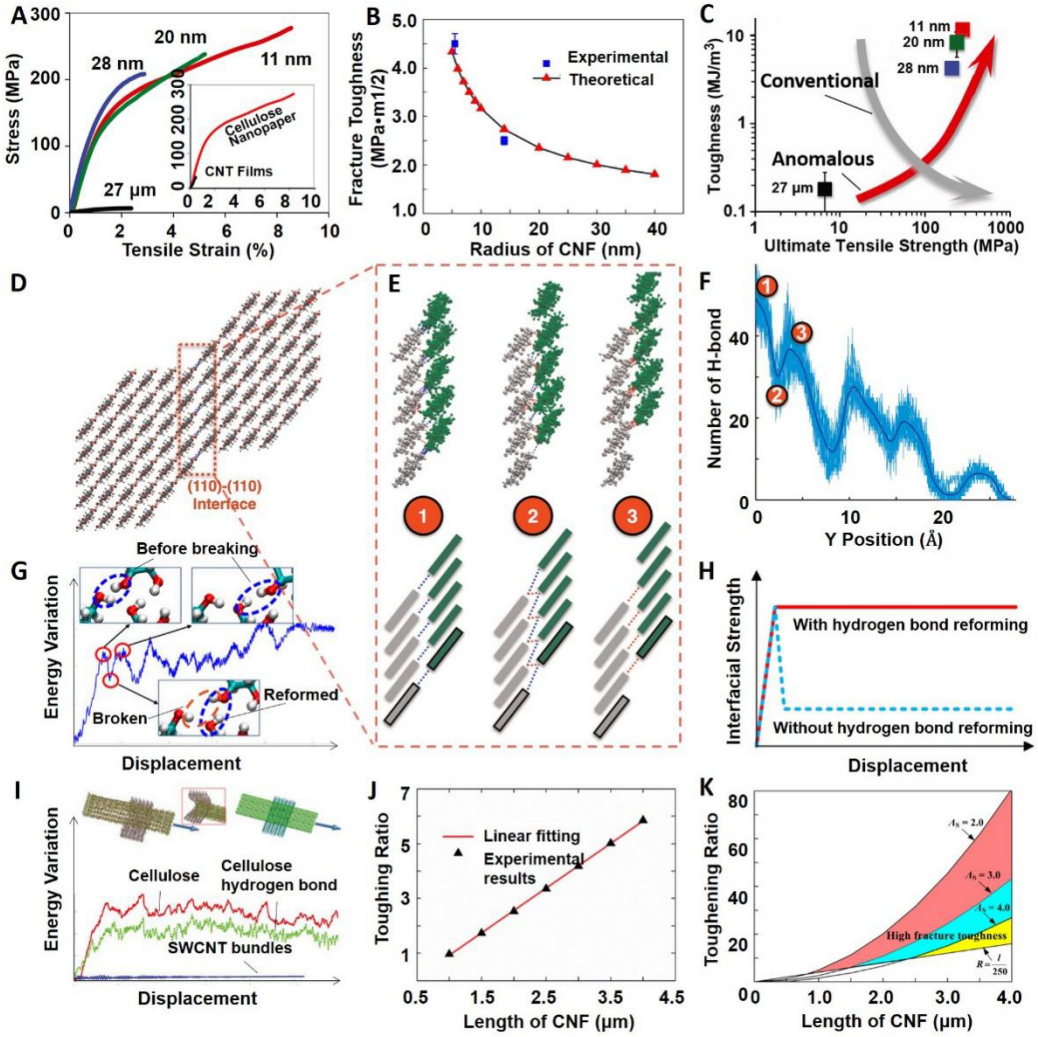

Figure 2. Mechanics of high mechanical performance of BC, which can achieve higher strength and higher toughness as the fiber diameter decreases. (A) Experimental stress-strain curves of cellulose nanopapers with different fiber diameters. The inset image compares the strength of cellulose nanopapers and CNT films made of nanomaterials with the same diameter (11 nm). (B) Fracture toughness of cellulose nanopapers relative to the radius of randomly oriented cellulose nanofibers (CNFs). (C) Relationship among the diameter, tensile strength, and toughness of nanopapers according to conventional and anomalous scaling law. (D) Alignment and connection of cellulose chains on the (110)-(110) interface. (E) Breaking and reformation of hydrogen bonds during shearing process at three locations, where cellulose chains are aligned at the beginning of the shearing (Location 1) through hydrogen bonds (blue), misaligned with hydrogen bonds breaking (blue), and the formation of new ones (Location 2) during the shearing and realigned (Location 3) by new hydrogen bonds (red) in the end at equilibrium. Variation of number (F) and energy (G) of hydrogen bonds during shearing at three locations. (H) Interface strength between cellulose nanofibrils under shear stress with (red) or without (blue) the reformation of hydrogen bond. (I) Energy variation relative to displacement of perpendicular sliding between two CNF fibers (green) or two single-walled carbon nanotube (SWCNT) bundles (blue). (J) Toughening ratio as a function of the CNF length. (K) Effect of cellulose diameter and length to fracture toughness. (A, C, G, I) Reproduced with permission[18]. Copyright 2015, National Academy of Sciences. (B) Reproduced with permission[23]. Copyright 2018, Elsevier. (D-F) Reproduced with permission[25]. Copyright 2015, Elsevier. (H, J, K) Reproduced with permission[26]. Copyright 2017, Elsevier.

original hydrogen bonds break and new ones reform [Figure 2F][25]. A local peak appears (Location 3) when new H-bonds form completely while one or few cellulose chains lose connection because of the dislocation and chain failure. Similar to the change in H-bond number, the interfacial energy varies with the sliding displacement [Figure 2G][18], beginning with a high value, declining along with the breaking of H-bonds, and climbing to the locally highest point as the H-bonds fully reform. The cycles of breaking and reforming

of hydrogen bonds continue with the sliding, during which the cellulose fibril overlap length decreases gradually as well as the number of H-bonds until the chains are pulled out entirely. With such cycles, the breaking process of self-healing H-bonds costs energy in a zigzag route, resisting the failure or fracture of the materials. It significantly dissipates energy, resulting in a much higher toughness. The pivotal contribution of the reformation of H-bonds to the higher fracture toughness of cellulose nanopaper is stressed by the cohesive models. The interfacial stress would drop significantly in the absence of reformation of H-bonds [Figure 2H][26], and the total potential energy varies nearly negligibly [Figure 2I][18], resulting in a reduced fracture toughness. Apart from the aforementioned factors, fracture toughness of nanopapers strongly depends on the length or aspect ratio of nanofibrils [Figure 2J][26]. To design a tough nanopaper, the aspect ratio of the nanofibers should be in the shadow region shown in Figure 2K[26]. Meanwhile, the high spatial density of interfacial hydrogen bonding because of neighboring cellulose chains in pure BC contributes to the high dissipation of energy as well, giving rise to enhanced toughness. Toughness benefits both strength and ductility. That is why natural BC is imparted with high strength as well as high ductility despite the high porosity.

Since massive hydrogen bonding sites along the BC fibril surface confer onto BC nanofibers extreme compatibility with functional nanomaterials by secondary bonding, BC-based nano-nano composites have emerged recently. The composite materials preserve the natural ecology and inherit the desirable properties of the initial BC with well-balanced flexibility, high strength, and porosity. On the other hand, to break through the limit of intact BC, discretization is applied to initial BC sheets or spheres to expand the species and application range of the nano-nano composites, e.g., conductive microfibers for supercapacitors and sensors. Although the intrinsic chemical and hydrogen bonds are damaged or rupture during dissociation, the reconstructed nano-nano materials based on the discrete BC fibers still perform better in strength, flexibility, and porosity compared with other functional composite materials or even plant cellulose-based composites which lack sufficient self-healing hydrogen bonds, purity, or DOP[26]. For most functional composite materials, hydrogen bonding sites or other types of strong bonds are not adequate to obtain tight connections between the components. With regards to plant cellulose, despite the identical chemical structure, it cannot perform as superlative as discrete BC fibers in mechanistic properties of the composites. The reason lies in the larger aspect ratio of BC nanofibers with higher anisotropy, benefiting the enhancement of hydrogen bonding sites, and relief of the defects of the composites[14]. This breaks the bottleneck on conveying properties of nano-cellulose to the bulk materials.

DESIGN STRATEGY FOR BC-BASED NANO-NANO STRUCTURE

To meet requests of different fields, various tactics are explored to produce BC-based nano-nano composites. Four categories are summarized in this section.

In-situ biological self-assembly

Billions of years of biological evolution has given birth to profoundly mysterious natural creatures, whose abilities for producing materials is unreachable for artificial simulation or synthesis. They can construct hierarchical structures with favorable physicochemical properties and maintain the nanosize effect. Compared with conventional assembling methods, such as freeze-drying, vacuum filtration, templating, and interface-controlling, bio-assembly favors energy-saving, environmental-friendliness, low-cost, high productivity, and potential of scalability, becoming a significant strategy to explore novel structure and materials.

Taking advantage of growth characteristics of *Acetobacter Xylinum*, bio-assembly based on BC means functional nanomaterials are dispersed and built up during the bacterial cultivation. The biological assembly

method to get BC-based nano-nano structures could be subdivided into three categories: dynamic culture, membrane-liquid culture, and static culture.

Dynamic culture

In dynamic culture, cellulose is produced under shearing force of continuous shaking or stirring, during which cellulose ribbons entangle with each other forming a spheroidal structure. When combined with nanomaterials, under constant shaking and stirring velocity, BC nanofibers can be homogeneously generated and dispersed with nanomaterials evenly loaded in BC spheres. The morphology and structure of the BC-based nano-nano composites is influenced by the ratio of nanomaterials, shaking or stirring speed and culture time. Taking graphene oxide (GO) as an example, a GO concentration of less than 0.05 mg/mL would generate a distinct spherical skin-core structure with a GO/BC composite core and pure BC shell, whereas higher concentration but no more than 0.15 mg/mL leads to homogenous distribution of GO in the irregular-shaped composite bulk[27]. Further increase of the GO in the culture medium would lead to unstable and uncompacted fragmentary composites for insufficient cellulose to anchor the GO sheets. Therefore, the proper ratio of nanomaterials is crucial in manufacturing integrated structure. By improving shaking speed and shortening the culture time, resembling the structure of pure BC [Figure 3A and D], graphene sheets (Gr) are assembled along with the BC nanofibers, creating a regular honeycomb-like surface pattern [Figure 3B and E][28]. After carbonization, the unique structure remained in the sphere-like carbonized bacterial cellulose (SCBC) [Figure 3C and F], resulting in an enhanced high absorption quantity [Figure 3G] contributed by large cavities and ridges[28]. Meanwhile, since graphene (GE) nanosheets are distributed evenly in and entangle with the SCBC network [Figure 3E and F], SCBC/GE presents good elasticity with a nearly complete recovery (compression ratio: ~90%)[28]. The fabricating strategy is a cost-effective and simple protocol to create novel biocompatible BC-based nano-nano materials for flexible or wearable electronics.

Membrane-liquid culture

Although dynamic culture could develop well-dispersed BC-based nano-nano composites under appropriate conditions, the resulted products are always either spherical or fragments, which limits its application in the fields of functional sheets or large-scale continuous production. To solve this problem effectively, membrane-liquid culture, so-called spray culture, has been developed to create planar films with controlled size and thickness and well-dispersed nanomaterials[29-32]. During the intermittent spraying [Figure 4A][29], the thickness of BC films depends on spraying cycles and volume of the medium [Figure 4B][33]. In low magnitude, the morphology seems to be changed to layered structure as a result of the intermittent spraying action [Figure 4C][32], while a magnified image shows a typical leaf/vein-like structure [Figure 4D and E] with 2D GO evenly distributed and tightly bonded with 1D BC nanofibers by strong hydrogen bonding[29]. Meanwhile, the composites exhibit good flexibility, capable of being bent or folded without any damage [Figure 4F], as well as a high tensile strength (218 MPa) [Figure 4G][32]. Thanks to these good properties, the supercapacitor based on the composite electrodes performs well in the bending state [Figure 4H][30]. In this mode, the mechanical properties of GO/BC were facilitated tremendously, deriving from the close mechanical bundling of GO nanosheets and BC nanofibers, strong hydrogen bonding, and uniform distribution of GO. Despite the various advantages, the membrane-liquid culture method suffers drawbacks of the complex manufacturing process.

Static culture

Static culture overcomes the disadvantage of operational difficulty in membrane-liquid culture since the mode needs no extra steps after dispersion of the nanomaterials and incubation of the bacteria. Take the assembling process of bacteria or BC with Gr and GO sheets as an example here. Similar to the dynamic and

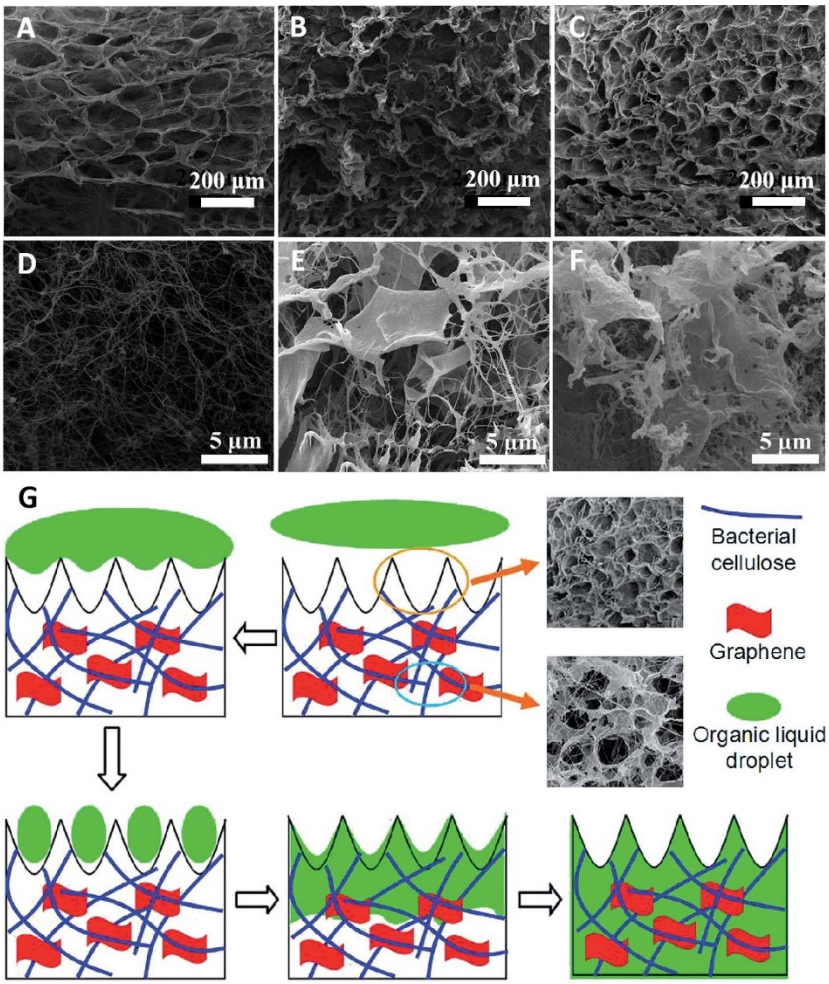

Figure 3. SEM images of surface (A-C) and internal (D-F): SCBC (A, D); Gr/SBC (B, E); and Gr/SCBC (C, F). (G) The absorption mechanisms showing the process by which liquids get into the Gr/SCBC. Reproduced with permission[28]. Copyright 2015, ACS.

membrane-liquid mode, during static culture, GO and Gr sheets were anchored continuously [Figure 5A] by initial BC nanofibers [Figure 5B], resulting in "spider-web" or "leaf-vein" structures [Figure 5C and D] with evenly dispersed nanosheets[34,35]. This unique structure could serve as a drug nanocarrier for *in vitro* drug release. Luo *et al.*[33] loaded ibuprofen on the porous nano-nano composites, demonstrating a non-Fickian diffusion mechanisms and better cell viability than biocompatible BC. After reduction, RGO/BC exhibited even higher cell proliferation as well as electrochemical activity[36]. To obtain the desired properties for specific applications, the addition of extra nanomaterials is a good choice. For example, well-dispersed SnO_2 nanoparticles inserted between the RGO/BC layers could enhance the electrochemical performance [Figure 5E-G][37].

Although various *in situ* methods have been attempted to assemble nanomaterials into BC aiming at exploiting the initial specific 3D structure of BC, the morphology of the resultant nano-nano composites tends to be disordered, differing widely with the regular honeycomb structure of pure BC. Guan *et al.*[38] investigated the mechanism [Figure 6A] and claimed that the concentration of nanomaterials plays a pivotal role in the way bacteria or bacterial cellulose bundles construct the nanomaterials. Either too little or excess nanomaterials would cause disordered or collapsed inner structure. Only under the optimized concentration of GO could the honeycomb-like morphology of BC be duplicated by the nano-nano

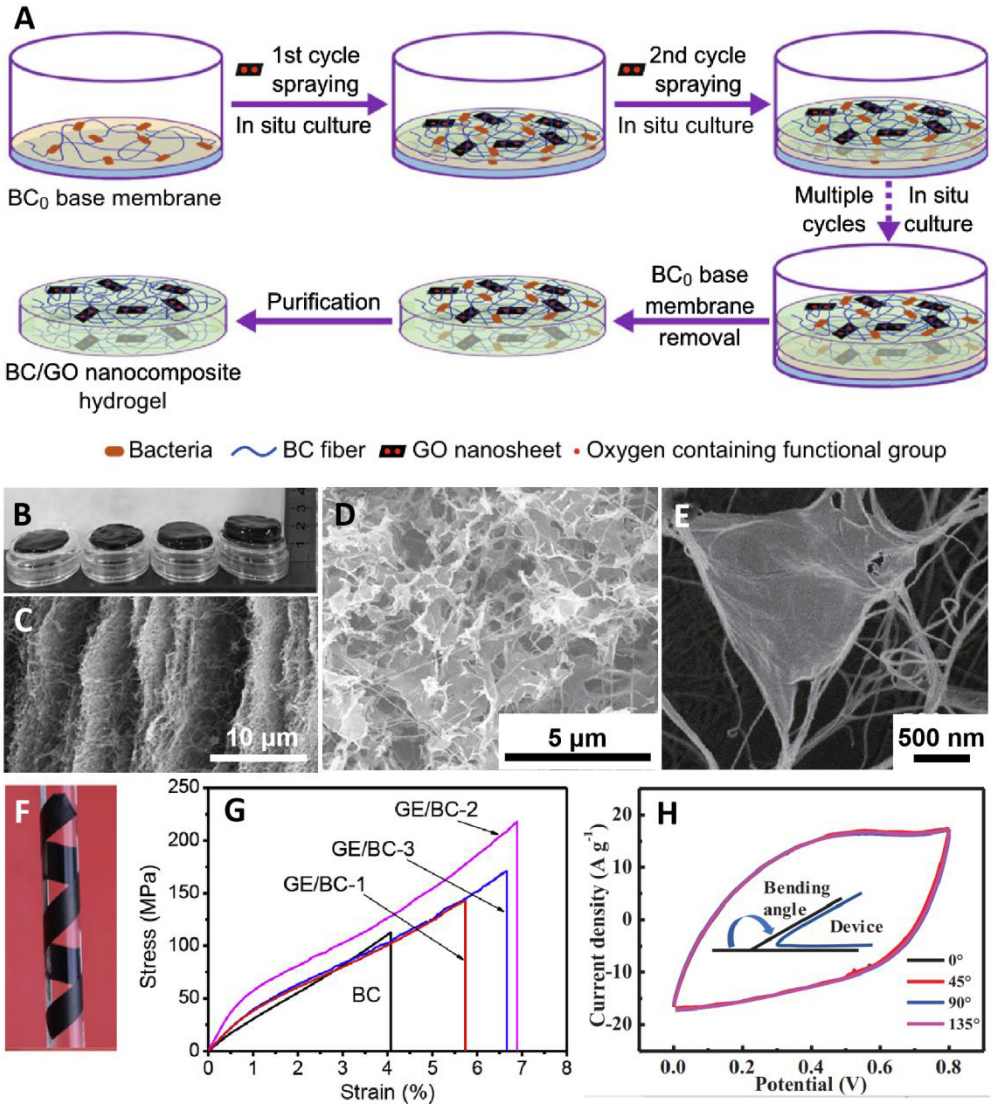

Figure 4. (A) Schematic illustration of the fabrication process of GO/BC nano-nano composite structure by membrane-liquid interface method. (B) Photos of Gr/BC samples with varying thickness. (C) The cross-sectional morphologies of freeze-dried Gr/BC showing layered structure. (D) SEM images taken from the surface layers of BC/GO. (E) Magnified SEM image of the "leaf and vein" nanostructure of BC/GO. (F) A photograph of a bent paper without damage. (G) Stress-strain curves of GE/BC sheets with different concentration of graphene. (H) Cyclic voltammogram curves of the CNF/GN electrode with various bending angles. (A, D, E) Reproduced with permission[29]. Copyright 2018, Springer. (B) Reproduced with permission[33]. Copyright 2018, Elsevier. (C, F, G) Reproduced with permission[32]. Copyright 2019, Elsevier. (H) Reproduced with permission[30]. Copyright 2018, Wiley.

composites [Figure 6B-D]. Despite the large number of pores, HGO/BC films are conferred with a high tensile strength of 204 MPa [Figure 6E] and exhibit excellent flexibility [Figure 6F]. The good balance between these properties imparts HGO/BC with good electrochemical performance for the shortened transport route of ions [Figure 6G], durability, and wearability[38].

Furthermore, with the biosynthesis strategy, integrative RGO-BC/BC bilayer films were generated with one dark brown GO-BC layer and one pure white BC layer [Figure 7A and B] because of the aerobiotic nature of *Acetobacter Xylinum*[39]. Notably, the two layers share the same fiber network, connected tightly through abundant natural strong BC nanofibers, as highlighted by the white dashed line in Figure 7C[39]. Based on

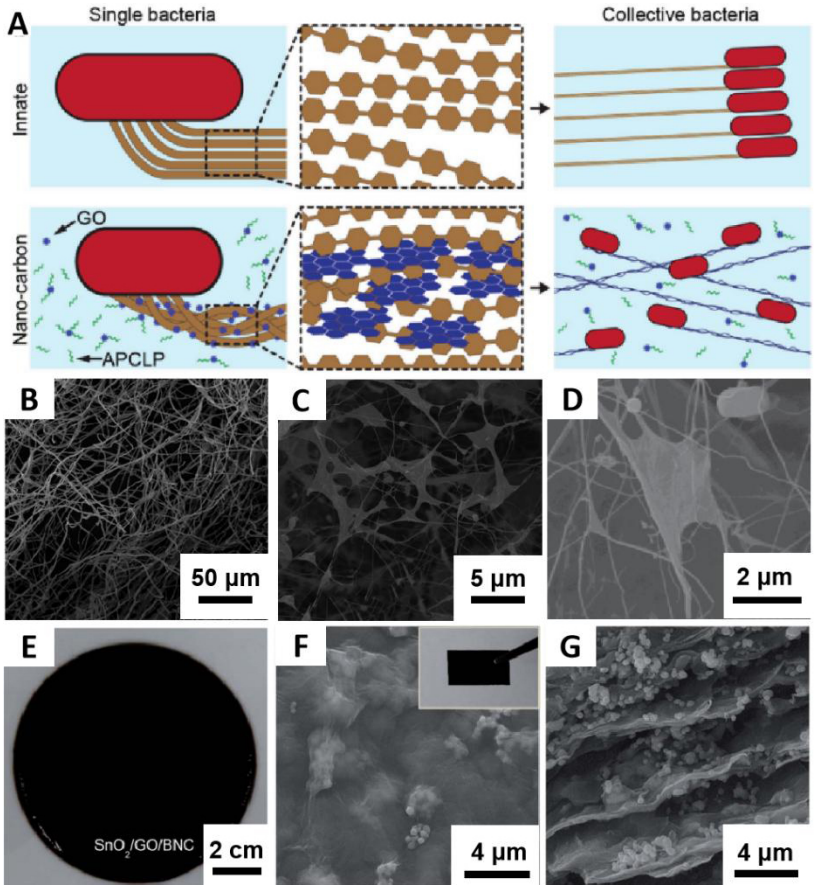

Figure 5. (A) The proposed mechanisms for bacterial cellulose synthesis in the absence (top) and presence (bottom) of nanocarbon flakes in the culture medium. SEM micrographs of nanocomposites: BC (B); Gr/BC (C); and GO/BC (D). (E) Photograph of the SnO_2 /GO/BNC hydrogel. (F) SEM image of the top surface of the SnO_2/GO/BNC. The inset shows the digital image of the SnO_2/GO/BNC film. (G) Cross-sectional SEM image of the SnO_2/GO/BNC. (A) Reproduced with permission[34]. Copyright 2019, Elsevier. (B-D) Reproduced with permission[35]. Copyright 2014, Wiley. (E-G) Reproduced with permission[37]. Copyright 2018, RSC.

this, i.e., compressible porous BC acting as the dielectric layers [Figure 7D], capacitive RGO-BC/BC sensors have good durability after thousands of bending cycles [Figure 7E][39].

Static culture features simple preparation, requires less labor, and is energy saving. The resultant nano-nano composites exhibit planar sheets of a controlled thickness (a few millimeters to several centimeters) with a regular honeycomb-like interior structure. For the maintenance of the compact network of BC, the composites possess excellent mechanical properties. The flexible, porous, high strength, and compatible BC-based nano-nano composites have been explored widely for application in the fields of supercapacitors, liquid purification, drug release, *etc*.[28,30-32,37,40-42]. However, one of the shortcomings of static culture for certain nanomaterials with relatively high density or that are difficul to disperse in culture medium is that nanomaterials would settle or even aggregate without the disturbance of external forces, causing uneven distribution of the functional materials in the network of BC[43]. Another drawback lies in the limitation of the shape of BC in static culture, usually plane sheets, and the requirement of a static state avoiding any disturbance as well as no biotoxicity of nanomaterials.

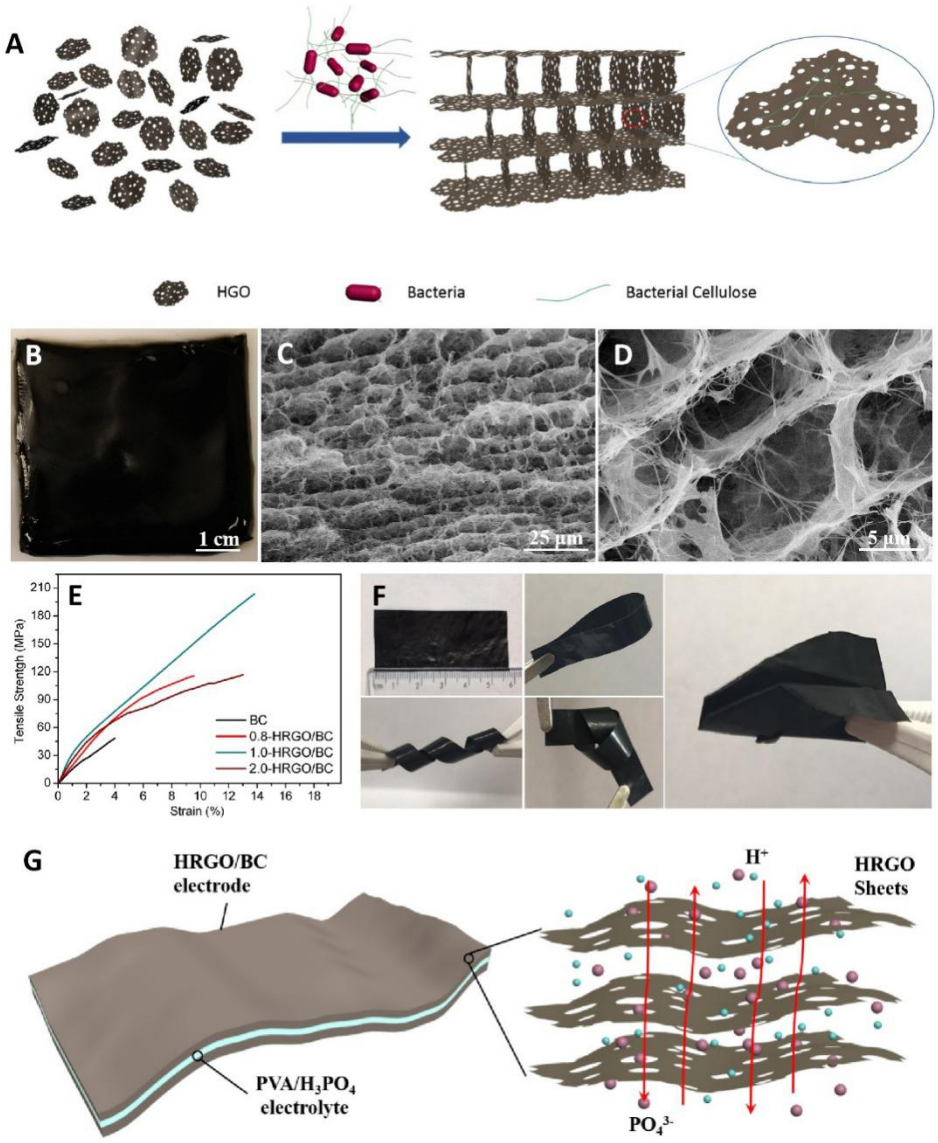

Figure 6. Optimized bio-assembly of GO using an *in situ* method. (A) Preparation process of GO/BC nano-nano composites. Digital photography of wet sheets (B) and cross-sectional scanning electronic microscope (SEM) views (C, D) of freeze-dried films for 1.0-HRGO/BC. (E) Mechanical performance of HRGO/BC membranes compared with BC films. (F) Optical images of flat-wise, bent, twisted, knotted, and folded 1.0-HRGO/BC films. (G) Schematic illustration of a sandwich-structure supercapacitor based on HRGO/BC nano-nano composites and the mechanism processing of electronic ions going across the pores in HRGO sheets. The red arrows refer to the ion transport pathways. (A-G) Reproduced with permission[38]. Copyright 2019, Elsevier.

Reconstruction

The reconstructing method is a favorable strategy to overcome the problem of uneven distribution of nanomaterials, shapes, and strict prerequisites in static culture. The process starts with the disintegration of 3D BC bundles or network into 1D BC nanofibers and follows with its hierarchically ordered reassembly under certain conditions, such as freeze-drying, hydrothermal state, *etc*.

To cleave the strongly bonded BC interpenetrating network into single fibers, high pressure homogenization is necessary. Acting as the adhesion agent, mechanically smashed BC fibers could connect 0D, 1D, and 2D nanomaterials to construct nano-nano composites, such as zein[44], aramid nanofibers[45],

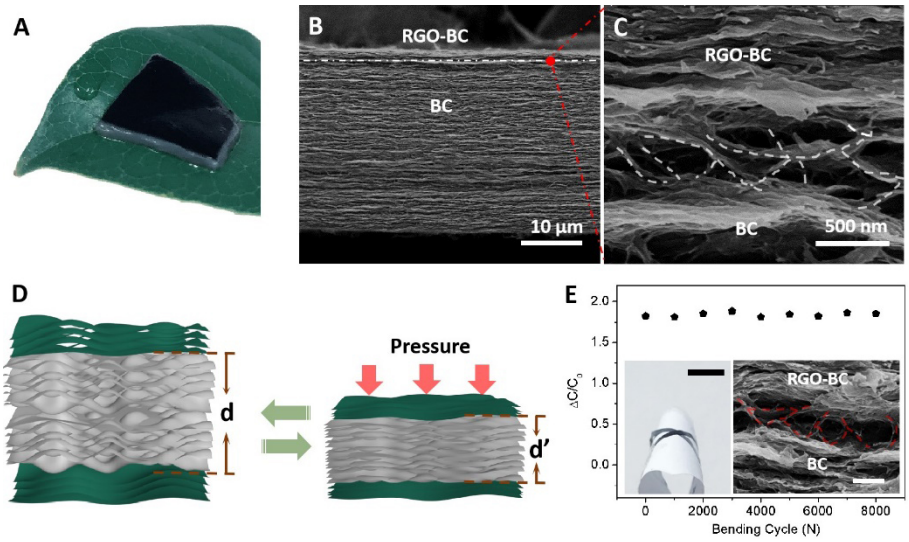

Figure 7. (A) A digital photograph of RGO-BC/BC bilayer hydrogel sheets. A cross-sectional FESEM image of dried RGO-BC/BC films (B) and interface of an RGO-BC/BC bilayer film with the connection of BC nanofibers (C). (D) Working mechanism of the pressure sensor based on RGO/BC films with BC layers as the dielectric layer. (E) Bending stability of the RGO-BC/BC pressure sensor. The curve radius is ~6 mm. The inset images indicate the bending process (left, scale bar = 1 cm) and the interface connection after 8000 bending cycles (right, scale bar = 500 nm). (A-E) Reproduced with permission[39]. Copyright 2020, Springer.

CNTs[46,47], GO[48,49], MXene[50,51], *etc.*, applied in the fields of supercapacitors, antimicrobial dressings, liquid absorption, and so on. 0D nanomaterials adhere on the surface of BC fibers [Figure 8A], while 1D nanomaterials intertwine with them due to the similar size, forming a network [Figure 8B and C][44,46]. However, a totally different morphology is presented when 2D nanomaterials are combined with BC nanofibers [Figure 8D][52]. Instead of the regular honeycomb-like structure in the in situ culture, the GO/BC aerogels by reconstruction have irregular pores but still exhibit an interpenetrating 3D network. BC nanofibers play key roles in the stable and uniform dispersion of GO nanosheets through spatial occupation between ruffly GO nanosheets aligned at random. Similarly, BC could suppress the MXene nanosheets' agglomeration or restacking and transfer densely stacked MXene into 3D porous microstructure [Figure 8E-G][51]. Abundant pores benefit the storage of electrolyte and shortening of the electrolyte ions' transport pathway. Due to the interconnected MXene nanosheets assembled by reticular or intertwined BC nanofibers, MXene/BC presents good mechanical properties and electrical conductivity.

For the nanosize effect and numerous hydroxide radicals, BC fibers tend to entangle together in water. To get a stable suspension, 2,2,6,6-tetramethylpiperidine-1-oxyl (TEMPO), a water-soluble and stable nitroxyl radical, is used to oxide the BC fibers[3,53-55]. TEMPO-oxidized bacterial cellulose (TOBC), which is highly charged, repulses each other efficiently for the electrostatic force, resulting in a stable well-dispersed colloid with individual nanofibrils in water[56]. Besides, the amphipathy derived from the hydrophobic lattice plane (200) and hydrophilic anion contributes to the dispersity of TOBC nanofibers[57]. Besides loading, TOBC can disperse nanomaterials with high agglomeration. After introducing BC nanofibers into the CNT dispersed solution, the CNTs' dispersibility is obviously improved and few aggregations can be observed, which indicates that completely individualized BC nanofibers dispersed in water could act as a dispersing agent for CNTs. TOBC has been proven to serve as dispersing agent for agglomerative nanomaterials[57-59]. For example, Yao *et al.*[57] introduced TOBC to a CNT suspension, resulting in obviously enhanced dispersibility with few CNT aggregations. After drying, a loose and porous structure is shaped with conductive nanomaterials or polymers covering along or connecting with TOBC nanofibers, generating a continuous conductive network. With TOBC as the strong backbone, the composites have high strength.

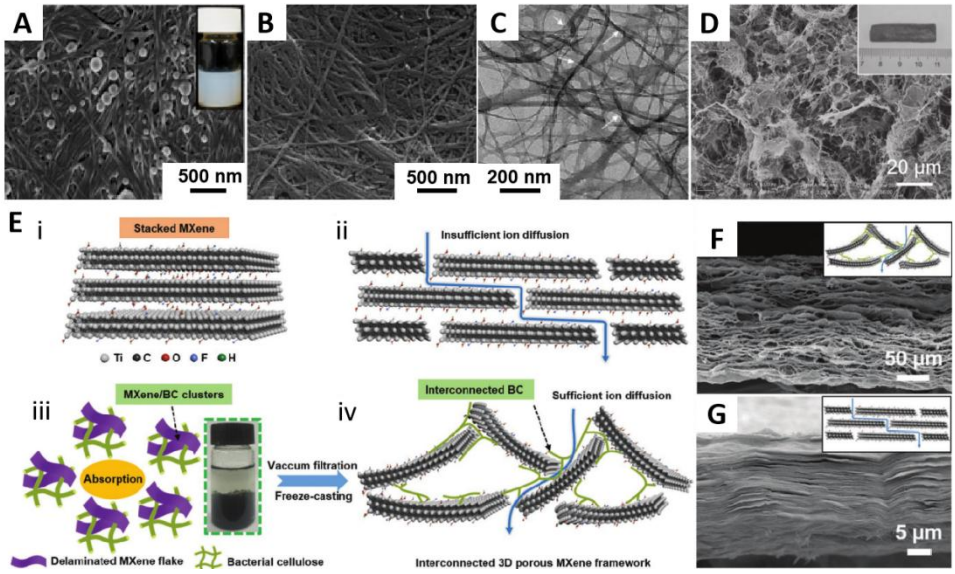

Figure 8. (A) SEM images and inset photographs of the homogeneous suspensions of BC-ZN systems. SEM (B) and TEM (C) images of CNT-BC. The white arrow refers to CNT. (D) SEM images of RGO/CNF aerogel. (E) Schematic illustration of the scheme design of porous MXene ($Ti_3C_2T_x$) architecture: (i) stacked MXene structure; (ii) ionic transport pathway in stacked MXene film; (iii) formation principle and photograph display of MXene/BC composites; and (iv) MXene/BC film structure and ionic transport pathway in 3D porous MXene framework. Cross-section images of MXene/BC film (F) and pure MXene film (G). (A) Reproduced with permission[44]. Copyright 2020, ACS. (B, C) Reproduced with permission[46]. Copyright 2020, Elsevier. (D) Reproduced with permission[52]. Copyright 2017, Wiley. (E) Reproduced with permission[51]. Copyright 2019, Wiley.

The pores and conductive pathway provide continuous binary channels for electrons and ions to transport[60,61]. These properties are ideal for high-performance supercapacitors.

Silver nanowire (AgNW), as a 1D metal nanomaterial, performs well in electrical conduction. When dispersed by TOBC and modeled with wet-spinning, AgNWs are shaped into unobtrusive fibers, capable of sensing tactile and proximity signals [Figure 9A][59]. TOBC presents its superiorities here in super-small diameter and super-large length. For the high aspect ratio, the size of TOBC resembles that of AgNW so that it can entangle with TOBC evenly and tightly. After quick double diffusion and evaporation of acetone, TOBC fibers shrink sharply, forming homogeneously distributed hierarchically porous morphology [Figure 9B and C][59]. AgNW-BC fibers present high tensile strength [Figure 9D] and sewability [Figure 9E] thanks to the high strength and ductility of the TOBC fibers[59]. With diagonal AgNW-BC fibers attached onto a choker, the AgNW-BC choker sensors could recognize different pronunciations [Figure 9F][59]. It is also available to detect heartbeat and vocal pulses, easily stitching the fibers into garments. Apart from that, the fiber sensor is able to detect the location of remote objects in two and three dimensions [Figure 9G and H][59]. The realization of such favorable bimodal function of AgNW-BC fibers relies on the balance of the inner porous structure, good mechanical performance, and flexibility, as well as high conductivity and instinct fiber nature. Thus, AgNW-BC fibers show extreme potential in smart, comfortable, and fashionable wearables.

Dispersing 2D GO nanosheets into an ionic liquid, TOBC could be made into high-fidelity bioelectronic artificial muscle, performing better in actuation compared with that of mechanically smashed BC nanofibers. It derives from carboxylic acid groups as proton donators providing abundant protons and larger ion exchange sites and surface area as well as stronger interfacial coupling[56]. When loading 0D nanoparticles, carboxyl on TOBC as a carrier can combine tightly with the alcoholic hydroxyl group

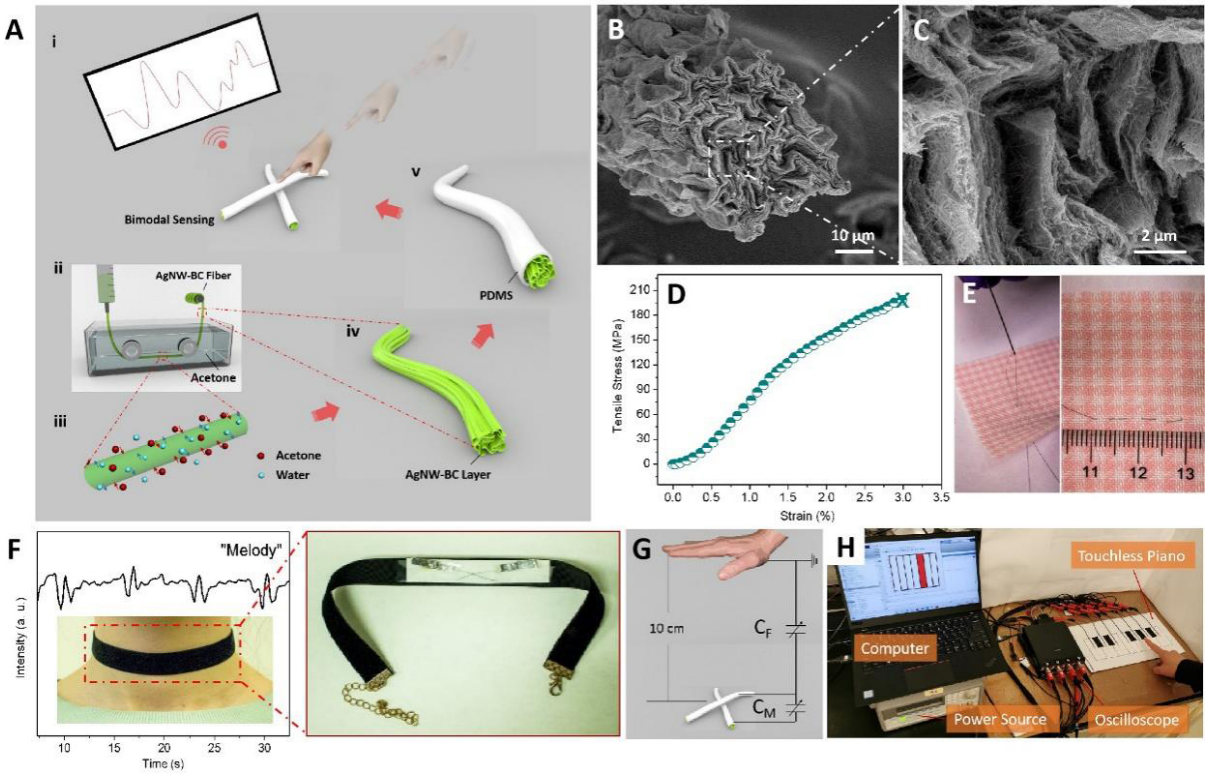

Figure 9. (A) Fabricating process of the AgNW-BC/PDMS bimodal platform. (B) Cross-sectional SEM images of AgNW-BC fiber, the enlarged inner porous structure of which is shown in (C). (D) Stress-strain curve of AgNW-BC fiber. (E) Threaded AgNW-BC fiber (left) impaled on cloth (right). (F) A choker sensor responding to the pronunciation of "melody". (G) Schematic scenario of touchless sensing of a single sensor. (H) Real scene of a touchless piano, played with one hovering human finger. (A-H) Reproduced with permission[58]. Copyright 2020, ACS.

through hydrogen bonding. When the obtained composites act as electrodes in Li-ion batteries, because of the tight bond of nanoparticles with TOBC backbone and high mechanical strength of TOBC, not only will the volume change of electrodes be alleviated and structural integrity improved, but the sustainable flexibility of the electrode during long-term usage is ensured as well, leaving out cumbersome metal current collectors[60].

Despite the reduction in the length and molar mass of CNF[62,63], TOBCs possess high specific moduli and tensile strengths[64-66], since TEMPO only breaks down part of the amorphous domains with no harm incurred to the crystalline ones and the high DOP ensures the high length of the bacterial nanofibers. Different from the *in situ* culture, in which the morphology of the resultant BC gels is limited to sheets, spherality/flocs and the nanomaterials should be strictly biocompatible, reconstruction is much more flexible and controllable with regard to the shapes and inner structure of the products and types of the additive, and much time can be saved based on the commercial pure BC.

Template inducing

Based on the initial 3D spatial network of BC, the template-inducing method could insert nanomaterials into the space between nanofibers or attach them onto the surface of fibers uniformly through extraction filtration, soaking, or *in situ* reaction. The steric and regulating effect of the 3D interpenetrating network of BC plays a key role in controlling the size, distribution, apparent condition, and structure of nanomaterials by intervening in the kinetic process of manufacturing systems, ensuring the homogeneity of morphology

and periodism of the structure. Natural BC sheets, as the skeleton, provide a coherent nanonetwork, benefiting the favorable properties such as high specific surface area, conductivity, mechanical strength, and so on[67,68]. By simple filtration [Figure 10A], nanomaterials could be filled and dispersed on one side of the BC nanonetwork while the other side remains pure BC under certain filtrating time and power as well as at a certain amount and concentration of nanomaterials [Figure 10B][69]. The integrated BC/d-$Ti_3C_2T_x$ (BC/MXene or BX) film is not only transparent and ultralight but also extremely flexible, capable of being folded into a paper plane [Figure 10C]. Meanwhile, BX films exhibit sufficient mechanical strength and toughness for wearable electronics, which increase with the increase in the amount of MXene [Figure 10D]. The highest mechanical strength, toughness, and Young's modulus reach ~532.87 MPa, ~31.14 $MJ \cdot m^{-3}$, and ~8.26 GPa, respectively, due to the effective interlocking effect of BC with 2D MXene nanosheets through strong interactions. The good electrical stability and durability of BX films were demonstrated by bending test, the influence of which on the resistance variation is neglectable [Figure 10E]. BX films present good wearability due to good air permeability and high subjective comfort level based on high scores graded by 30 respondents in different aspects [Figure 10F]. For MXene and BX layers reflecting repeatedly and adsorbing abundant free electrons[70], the BX films are imparted with excellent electromagnetic interface (EMI) shielding ability [Figure 10G]. With the increase of the amount of MXene, the EMI shielding effectiveness climbs and reaches ~20.2 dB with an SSE/t value of ~69,455.2 $dB \cdot cm^2 \cdot g^{-1}$ [Figure 10H], sufficient for commercial electronics demanding 99% attenuation.

To make nanomaterials fully distributed in the whole film, a soaking precursor-reduce/oxidize process is adopted to construct even composites [Figure 11A][71]. Abundant hydrogen bonds on the surface of BC nanofibers can densely and uniformly anchor the precursor of nanomaterials. Meanwhile, the 3D nano-skeleton of BC overcomes the dipole force between nanomaterials, preventing agglomeration of the densely oriented nanomaterials. In this way, an ideal flexible BC-based nano-nano composite structure is obtained by loading superdense and uniformly dispersed nanomaterials, including nanoparticles (polymers[72], metal[73-75], metallic oxide[76], carbide, or sulfide[71,77-87]) and nanoclusters[88]. The size, distribution, and morphology of nanomaterials could be adjusted by the number of functional groups and concentration of ions in the precursor solution. The template-induced BC-based nano-nano composites maintain the initial 3D porous network [Figure 11B] that can absorb liquid, store electrolyte, and transport electrons and ions[71]. Compression forces them into highly loaded nanopapers [Figure 11C][71], with potential in the fields of antibacterial dressings[75,89], drug delivery systems[86], bio-sensing[73], nerve scaffolds[72], desalination of seawater[77], energy storage[79], electromagnetic shielding[71,85], and others. The nanoparticle structure is adjustable, and its size increases gradually to 120 nm [Figure 11D] by controlling the concentration of the $FeSO_4/CoCl_2$ solution and narrowly distributed in a range of 30%-40%. The composite aerogels exhibit unexpected flexibility, which can be repeatedly bent to 180° without apparent damage [Figure 11E and F]. Meanwhile, the nanocomposites have large coercivities [Figure 11G] and fully recover their properties after measured at 200 °C (Figure 11G, inset), demonstrating the high-temperature stability of the composite aerogels. As mentioned above, dried aerogels, especially solvent swollen gels and magnetic nanoparticle-containing solvent swollen ferrogels that are responsive and able to actuate to magnetic, are typically brittle[90,91]. However, for high strength and toughness, such BC-based magnetic aerogels are demonstrated to be capable of being magnetically actuated and reversibly absorbing water by bending themselves and then recovering their initial shape repeatedly [Figure 11H][71].

The templating method features simple experimental setup, ease of operation, controllable morphology, and wide application. Despite such advantages, one shortcoming lies in the composites being limited by the morphology of initial BC, such as its thickness, shape, structure, and so on.

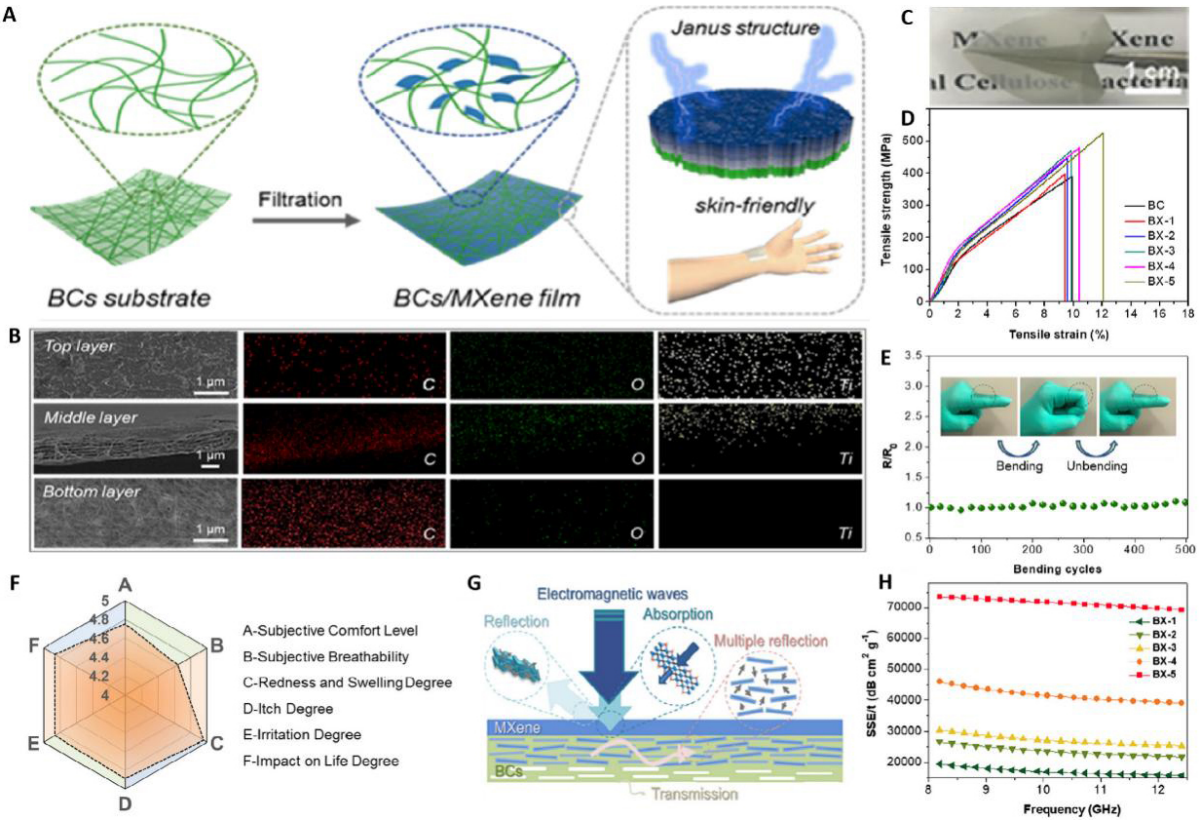

Figure 10. (A) Schematic of the BC/MXene film preparation. (B) SEM and energy dispersive X-ray spectrometers (EDS) elemental mapping images reveal the BC/MXene films with Janus structure. (C) A photograph of a folded BC/MXene film. (D) Mechanical properties of the BC/MXene films with different concentrations of MXene. (E) Electrical resistance stability of BC/MXene films worn on a human index finger bent at different angles. (F) Comfort level of BC/MXene films in the form of a six-dimensional analysis framework. (G) Schematic illustration of BC/MXene films shielding electromagnetic interface (EMI) wave. (H) Specific shielding effectiveness (SSE/t) value of the BC/MXene (BX) films in the X-band region. (A-H) Reproduced with permission[69]. Copyright 2021, Elsevier.

Carbonization

Construction of carbonized-BC (CBC)-based nano-nano composites through carbonization starts with the removal of micromolecules, such as CO, CO_2, methanol, and acetic acid, putting dried BC under the protection of inert gases in a high-temperature environment, following the composition of nanomaterials. An alternative method could be directly pyrolyzing the BC nano-nano composites[92]. Compared with the initial BC, the size of CBC reduces in all three dimensions, resulting in 85% shrink ratio, a decrease in density from 7-10 to 3-6 mg/cm^3[93], and 10-20 nm width nanofibers (initial: 20-50 nm) but maintaining a stable porosity of about 99.6%[92]. After carbonization, the carbon element separates out, leading to the capability of transporting electrons through the carbon backbone. The critical factor affecting the conductivity of CBC is the pyrolysis temperature. Above 1000 °C, the conductivity reaches up to 0.2 S/cm[92]. Another benefit of carbonization is the reversible compressibility, since the disappearance of hydroxy for the removal of hydrogen atoms weakens hydrogen bonding[92]. Thus, CBC aerogels deriving from BC consisting of a 3D interpenetrating nanonetwork are conferred with particular physical properties, such as low density, high conductivity, high aspect surface area, and reversible compressibility[93-95]. Manufacturing of CBC aerogels features simplicity of operation, low-cost, environmental-friendliness, and scalability, solving the problems that currently exist in the preparation of carbon-based aerogels. Such problems include the toxicity of the precursor, complexity of preparation equipment, difficulty in large-scale fabrication, *etc.*[93].

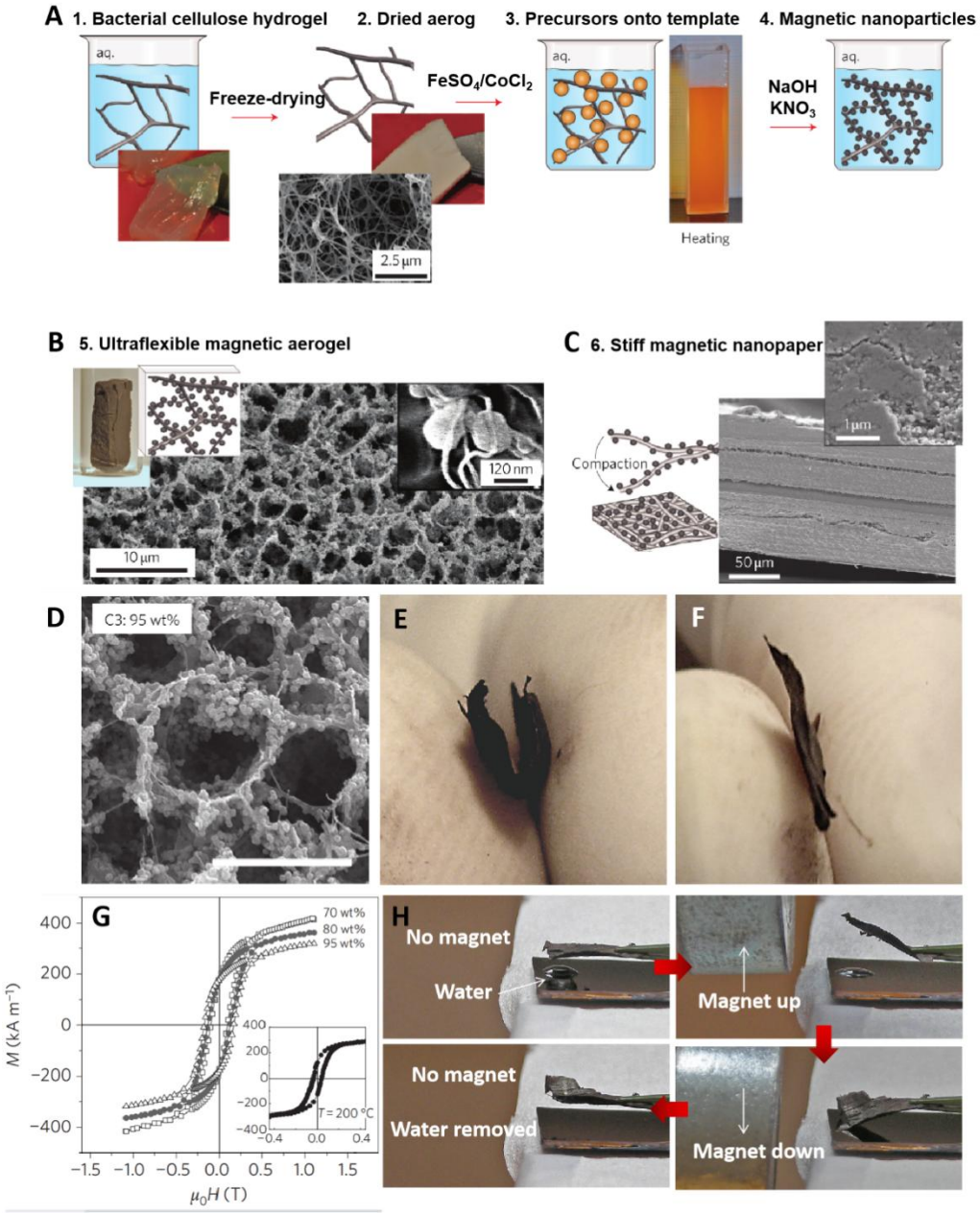

Figure 11. (A) Synthesis of elastic aerogel magnets. (B) SEM image of a 98% porous magnetic aerogel containing cobalt ferrite nanoparticles after freeze-drying. (Right inset) Nanoparticles surrounding the nanofibrils. (Left insets) Photograph and schematic of the aerogel. (C) SEM image of a stiff magnetic nanopaper obtained after drying and compression. (Inset) Higher magnification image. (D) SEM image of one BC-based magnetic sample (C3) with 95 wt% of particles. Scale bars is 4 mm. Photographs of the magnetic aerogel being bent € and after being folded (F) in the dried state. (G) Magnetic hysteresis loops of BC/$CoFe_2O_4$ aerogels. The inset image shows the hysteresis loop of BC/$CoFe_2O_4$ aerogels at T = 200 °C. (H) Actuation process of the magnetic aerogel responding to the magnet where it bends and absorbs the water droplet and then recovers its initial state upon removal of the magnet. (A-H) Reproduced with permission[71]. Copyright 2010, Nature.

CBC-based nano-nano composites have been widely applied in the fields of electromagnetic shielding[96], catalytic hydrogen evolution[97,98], supercapacitor[99], and Li-ion battery[100,101]. CBC is crucial to the high energy density and power density of the asymmetric supercapacitors[88]. Chen *et al.*[88] studied the carbonization of BC [Figure 12A-C] and constructed supercapacitors with CBC-based nano-nano

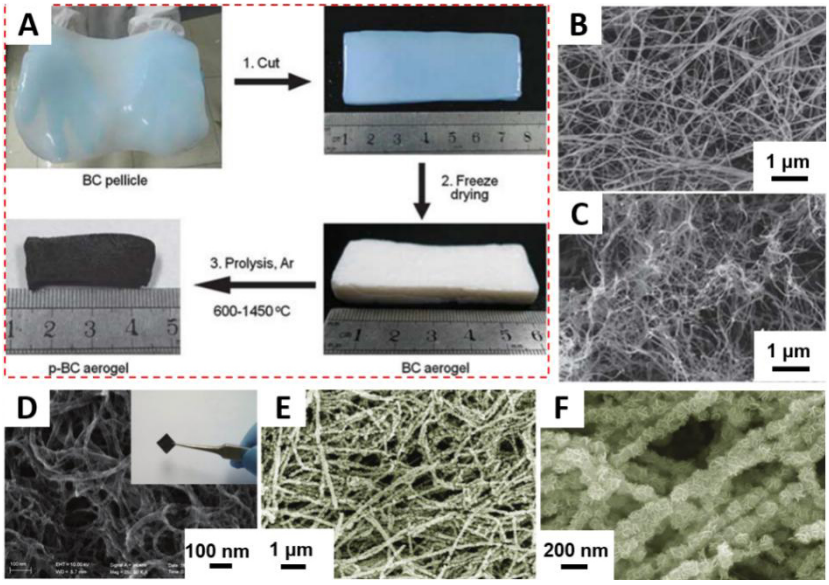

Figure 12. (A) The fabrication process of CBC materials: (1) A large-sized BC pellicle (200 × 230 × 3 mm^3) was cut into the desired shape with a sharp blade. (2) After freeze-drying of the wet BC pellicles, the ultralight BC aerogel was obtained. (3) Further pyrolysis treatment of the BC aerogel under flowing argon produced the black p-BC aerogel. SEM images of hybrid nanofibers: BC (B); CBC (C); CBC@MnO_2; (D) hybrid nanofibers; and CBC/$MoSe_2$ (E, F). The inset image in (D) is the photograph of the CBC@MnO_2. (A-C) Reproduced with permission[92]. Copyright 2012, Nature. (D) Reproduced with permission[88]. Copyright 2013, Wiley. (E, F) Reproduced with permission[98]. Copyright 2016, Wiley.

composites as their electrodes. CBC can also serve as reductant to reduce MnO_4^- into MnO_2 nanoparticles[88]. The 3D network of initial CBC remained in the CBC@MnO_2 composites [Figure 12D][88]. Apart from the role of reducing and as a framework, CBC as the conductive substrate benefits the quick transport of ions and electrons. The tight bonding and synergistic effect of MnO_2 nanoparticles and CBC nanofibers effectively shortens the transport path of electrolyte ions as well as provides a fast reversible faradic redox reaction, indicating the potential of CBC as an ideal candidate material for supercapacitors. For the catalytic hydrogen production, CBC skeleton forces $MoSe_2$ nanoparticles to three-dimensionally disperse evenly [Figure 12E and F] and prevent the aggregation of $MoSe_2$ nanoparticles, resulting in more effective active sites compared with those with no 3D framework[98]. Resembling the principle of supercapacitors, the porous network of CBC/$MoSe_2$ could not only store electrolytes but also obviously accelerate electron transport[98], bringing about a high catalytic efficiency as a consequence.

Doping heteroatoms, e.g., N, P, S, B, *etc.*, can enhance the properties of photoelectrocatalysis, supercapacitors, Li-ion batteries, and absorption of electromagnetic wave[102]. The hydrothermal method is often adopted to dope these heteroatoms, e.g., pyrolyzing BC coated with polymers, salt, or micromolecues rich in heteroatoms or putting in the corresponding gas, such as H_3PO_4[96], urea[97], PAN[99], and so on. Doping P on BC will widen the absorption spectrum range of the electromagnetic wave, and the absorption band can be adjusted between medium and high frequency[96]. N-doped CBC possesses more active sites, promoting the process of hydrogenation and thus improving the efficiency of hydrogen production[97]. Such flexible BC-based nano-nano composites with enhanced properties, e.g., conductivity, storage capability, catalytic ability, *etc.*, are promising in future flexible or wearable electronics.

CLOSING STATEMENTS AND FUTURE OUTLOOK

Increasingly severe environmental pollution issues of nonbiodegradable petroleum-based synthetic polymers promote the investigation and application of renewable biomass resources. Featuring versatile, unique, and superior characteristics, e.g., high strength, porosity, and flexibility, bacterial cellulose emerges in various technological and day-to-day areas, opening up a novel avenue to fulfill the growing requirements of modern life and technology.

In this progress report, we delineate the underlying mechanism elucidating the good balance among high strength, flexibility, and porosity of BC and BC-based functional nano-nano materials, which are supposed to conflict with each other. Seminal experimental and theoretical investigations elucidate the pivotal role of interfacial hydrogen bonds and the unique superiority (e.g., high purity, crystallinity, and aspect ratio of nanofibers) of BC for the remarkable properties of the BC-derived nanocomposites. The detailed account of the mechanism and ongoing examples show the large potential of BC and its nanocomposites in producing renewable electronics. Herein, the strategies for constructing desirable BC-based nanocomposites are proposed. Various tactics with distinguished features satisfy the growing special demands of high-performance flexible electronics.

Despite the fulfilled achievements, certain bottlenecks are encountered, classified into three categories. (1) Scientific problems: a better understanding of the factors affecting the properties of BC nanofibers and the mechanism of cell mutations vital to the BC production is still need. (2) Performance issues: the abundant hydrogen bond sites benefit the high performance of BC-based nano-nano composites but also cause the poor long-term durability and water/humidity resistance. Meanwhile, reliable and accurate characterizations of the composites are essential to standardize both laboratory and industrial production. (3) Economic matters: the advantageous properties (e.g., high DOP and degree of crystallinity and intact 3D nanonetwork) of BC and its nano-nano composites require careful production and purification, limiting their economic feasibility, which hinders their industrial exploration and application.

Future research and development of BC-based nano-nano materials should be directed to the fundamental scientific understanding of the formation of BC and its nanofibers, hydrophobic treatment, and high-efficiency production. Based on these efforts, the well-crafted design will broaden the application spectrum of BC-based nano-nano composites in high-performance areas as well as their generic use, allowing them to fulfill objectives in the midterm thanks to the biomass nature of BC.

DECLARATIONS

Authors' contributions

Designed and wrote the original draft: Guan F
Supervised, reviewed and revised the manuscript: Guo CF

Availability of data and materials

Not applicable.

Financial support and sponsorship

This work was financially supported by the National Natural Science Foundation of China (No. 52073138).

Conflicts of interest

Both authors declared that there are no conflicts of interest.

Ethical approval and consent to participate

Not applicable.

Consent for publication

Not applicable.

REFERENCES

1. Rochman CM, Browne MA, Halpern BS, et al. Policy: classify plastic waste as hazardous. *Nature* 2013;494:169-71. DOI PubMed
2. MacArthur E. Beyond plastic waste. *Science* 2017;358:843. DOI PubMed
3. Isogai A. Development of completely dispersed cellulose nanofibers. *Proc Jpn Acad Ser B Phys Biol Sci* 2018;94:161-79. DOI PubMed PMC
4. Zhu Y, Romain C, Williams CK. Sustainable polymers from renewable resources. *Nature* 2016;540:354-62. DOI PubMed
5. Kou H, Lu J, Li Y. High-strength and high-ductility nanostructured and amorphous metallic materials. *Adv Mater* 2014;26:5518-24. DOI PubMed
6. Gong J, Katsuyama Y, Kurokawa T, Osada Y. Double-network hydrogels with extremely high mechanical strength. *Adv Mater* 2003;15:1155-8. DOI
7. Zhang XF, Ma X, Hou T, et al. Inorganic salts induce thermally reversible and anti-freezing cellulose hydrogels. *Angew Chem Int Ed Engl* 2019;58:7366-70. DOI PubMed
8. Moon RJ, Martini A, Nairn J, Simonsen J, Youngblood J. Cellulose nanomaterials review: structure, properties and nanocomposites. *Chem Soc Rev* 2011;40:3941-94. DOI PubMed
9. Lee KY, Buldum G, Mantalaris A, Bismarck A. More than meets the eye in bacterial cellulose: biosynthesis, bioprocessing, and applications in advanced fiber composites. *Macromol Biosci* 2014;14:10-32. DOI PubMed
10. Ross P, Mayer R, Benziman M. Cellulose biosynthesis and function in bacteria. *Microbiol Rev* 1991;55:35-58. DOI PubMed PMC
11. Hirai A, Tsuji M, Horii F. TEM study of band-like cellulose assemblies produced by acetobacter xylinum at 4 °C. *Cellulose* 2002;9:105-13. DOI
12. Dahman Y. Nanostructured biomaterials and biocomposites from bacterial cellulose nanofibers. *J Nanosci Nanotechnol* 2009;9:5105-22. DOI PubMed
13. Maria LCS, Santos ALC, Oliveira PC, et al. Preparation and antibacterial activity of silver nanoparticles impregnated in bacterial cellulose. *Polímeros* 2010;20:72-7. DOI
14. Iguchi M, Yamanaka S, Budhiono A. Bacterial cellulose - a masterpiece of nature's arts. *J Mater Sci* 2000;35:261-70. DOI
15. Bäckdahl H, Helenius G, Bodin A, et al. Mechanical properties of bacterial cellulose and interactions with smooth muscle cells. *Biomaterials* 2006;27:2141-9. DOI PubMed
16. Vitta S, Thiruvengadam V. Multifunctional bacterial cellulose and nanoparticle-embedded composites. *Curr Sci* 2012;102:1398-405. DOI
17. Wu ZY, Liang HW, Chen LF, Hu BC, Yu SH. Bacterial cellulose: a robust platform for design of three dimensional carbon-based functional nanomaterials. *Acc Chem Res* 2016;49:96-105. DOI PubMed
18. Zhu H, Zhu S, Jia Z, et al. Anomalous scaling law of strength and toughness of cellulose nanopaper. *Proc Natl Acad Sci U S A* 2015;112:8971-6. DOI PubMed PMC
19. Ritchie RO. The conflicts between strength and toughness. *Nat Mater* 2011;10:817-22. DOI PubMed
20. Evans AG. Perspective on the development of high-toughness ceramics. *J Am Ceram Soc* 1990;73:187-206. DOI
21. Hofmann DC, Suh JY, Wiest A, et al. Designing metallic glass matrix composites with high toughness and tensile ductility. *Nature* 2008;451:1085-9. DOI PubMed
22. Launey ME, Ritchie RO. On the fracture toughness of advanced materials. *Adv Mater* 2009;21:2103-10. DOI PubMed PMC
23. Meng Q, Li B, Li T, Feng X. Effects of nanofiber orientations on the fracture toughness of cellulose nanopaper. *Eng Fract Mech* 2018;194:350-61. DOI
24. Ray U, Zhu S, Pang Z, Li T. Mechanics design in cellulose-enabled high-performance functional materials. *Adv Mater* 2021;33:e2002504. DOI PubMed
25. Sinko R, Keten S. Traction-separation laws and stick-slip shear phenomenon of interfaces between cellulose nanocrystals. *J Mech Phys Solids* 2015;78:526-39. DOI
26. Meng Q, Li B, Li T, Feng XQ. A multiscale crack-bridging model of cellulose nanopaper. *J Mech Phys Solids* 2017;103:22-39. DOI
27. Nandgaonkar AG, Wang Q, Fu K, et al. A one-pot biosynthesis of reduced graphene oxide (RGO)/bacterial cellulose (BC) nanocomposites. *Green Chem* 2014;16:3195-201. DOI
28. Wan Y, Zhang F, Li C, Xiong G, Zhu Y, Luo H. Facile and scalable production of three-dimensional spherical carbonized bacterial cellulose/graphene nanocomposites with a honeycomb-like surface pattern as potential superior absorbents. *J Mater Chem A* 2015;3:24389-96. DOI

29. Luo H, Dong J, Yao F, et al. Layer-by-layer assembled bacterial cellulose/graphene oxide hydrogels with extremely enhanced mechanical properties. *Nanomicro Lett* 2018;10:42. DOI PubMed PMC
30. Luo H, Xiong P, Xie J, et al. Uniformly dispersed freestanding carbon nanofiber/graphene electrodes made by a scalable biological method for high-performance flexible supercapacitors. *Adv Funct Mater* 2018;28:1803075. DOI
31. Wan Y, Yang S, Wang J, et al. Scalable synthesis of robust and stretchable composite wound dressings by dispersing silver nanowires in continuous bacterial cellulose. *Composites Part B* 2020;199:108259. DOI
32. Luo H, Xie J, Xiong L, Zhu Y, Yang Z, Wan Y. Fabrication of flexible, ultra-strong, and highly conductive bacterial cellulose-based paper by engineering dispersion of graphene nanosheets. *Composites Part B* 2019;162:484-90. DOI
33. Luo H, Dong J, Xu X, Wang J, Yang Z, Wan Y. Exploring excellent dispersion of graphene nanosheets in three-dimensional bacterial cellulose for ultra-strong nanocomposite hydrogels. *Composites Part A* 2018;109:290-7. DOI
34. Kim D, Park S, Jo I, et al. Multiscale modulation of nanocrystalline cellulose hydrogel via nanocarbon hybridization for 3D neuronal bilayer formation. *Small* 2017;13:1700331. DOI PubMed
35. Luo H, Xiong G, Yang Z, Raman SR, Si H, Wan Y. A novel three-dimensional graphene/bacterial cellulose nanocomposite prepared by in situ biosynthesis. *RSC Adv* 2014;4:14369-72. DOI
36. Jin L, Zeng Z, Kuddannaya S, Wu D, Zhang Y, Wang Z. Biocompatible, free-standing film composed of bacterial cellulose nanofibers-graphene composite. *ACS Appl Mater Interfaces* 2016;8:1011-8. DOI PubMed
37. Liu K, Jiang Q, Kacica C, Derami HG, Biswas P, Singamaneni S. Flexible solid-state supercapacitor based on tin oxide/reduced graphene oxide/bacterial nanocellulose. *RSC Adv* 2018;8:31296-302. DOI
38. Guan F, Chen S, Sheng N, et al. Mechanically robust reduced graphene oxide/bacterial cellulose film obtained via biosynthesis for flexible supercapacitor. *Chem Eng J* 2019;360:829-37. DOI
39. Guan F, Han Z, Jin M, et al. Durable and flexible bio-assembled RGO-BC/BC bilayer electrodes for pressure sensing. *Adv Fiber Mater* 2021;3:128-37. DOI
40. Jiang Q, Ghim D, Cao S, et al. Photothermally active reduced graphene oxide/bacterial nanocellulose composites as biofouling-resistant ultrafiltration membranes. *Environ Sci Technol* 2019;53:412-21. DOI PubMed
41. Luo H, Ao H, Li G, et al. Bacterial cellulose/graphene oxide nanocomposite as a novel drug delivery system. *Curr Appl Phys* 2017;17:249-54. DOI
42. Ye J, Guo L, Feng Y, et al. Fabrication of bacterial cellulose-based ATO-PPy nanocomposites as flexible conductive materials. *J Electron Mater* 2020;49:6686-94. DOI
43. Shah N, Ul-Islam M, Khattak WA, Park JK. Overview of bacterial cellulose composites: a multipurpose advanced material. *Carbohydr Polym* 2013;98:1585-98. DOI PubMed
44. Li Q, Gao R, Wang L, et al. Nanocomposites of bacterial cellulose nanofibrils and zein nanoparticles for food packaging. *ACS Appl Nano Mater* 2020;3:2899-910. DOI
45. Yang Y, Huang C, Gao G, Hu C, Luo L, Xu J. Aramid nanofiber/bacterial cellulose composite separators for lithium-ion batteries. *Carbohydr Polym* 2020;247:116702. DOI PubMed
46. Fang D, Zhou J, Sheng L, Tang W, Tang J. Juglone bonded carbon nanotubes interweaving cellulose nanofibers as self-standing membrane electrodes for flexible high energy supercapacitors. *Chem Eng J* 2020;396:125325. DOI
47. Nie X, Lv P, Stanley SL, Wang D, Wu S, Wei Q. Ultralight nanocomposite aerogels with interpenetrating network structure of bacterial cellulose for oil absorption. *J Appl Polym Sci* 2019;136:48000. DOI
48. Ma L, Bi Z, Zhang W, et al. Synthesis of a three-dimensional interconnected oxygen-, boron-, nitrogen-, and phosphorus tetratomic-doped porous carbon network as electrode material for the construction of a superior flexible supercapacitor. *ACS Appl Mater Interfaces* 2020;12:46170-80. DOI PubMed
49. Liu Y, Zhou J, Zhu E, Tang J, Liu X, Tang W. Facile synthesis of bacterial cellulose fibres covalently intercalated with graphene oxide by one-step cross-linking for robust supercapacitors. *J Mater Chem C* 2015;3:1011-7. DOI
50. Zhu J, Shi R, Liu Y, et al. 3D interwoven MXene networks fabricated by the assistance of bacterial celluloses as high-performance cathode material for rechargeable magnesium battery. *Appl Surf Sci* 2020;528:146985. DOI
51. Wang Y, Wang X, Li X, et al. Engineering 3D ion transport channels for flexible MXene films with superior capacitive performance. *Adv Funct Mater* 2019;29:1900326. DOI
52. Li C, Wu ZY, Liang HW, Chen JF, Yu SH. Ultralight multifunctional carbon-based aerogels by combining graphene oxide and bacterial cellulose. *Small* 2017;13:1700453. DOI PubMed
53. Isogai A, Saito T, Fukuzumi H. TEMPO-oxidized cellulose nanofibers. *Nanoscale* 2011;3:71-85. DOI PubMed
54. Isogai A. Wood nanocelluloses: fundamentals and applications as new bio-based nanomaterials. *J Wood Sci* 2013;59:449-59. DOI
55. Isogai A, Hänninen T, Fujisawa S, Saito T. Review: catalytic oxidation of cellulose with nitroxyl radicals under aqueous conditions. *Prog Polym Sci* 2018;86:122-48. DOI
56. Kim S, Jeon J, Kim H, Kee CD, Oh I. High-fidelity bioelectronic muscular actuator based on graphene-mediated and TEMPO-oxidized bacterial cellulose. *Adv Funct Mater* 2015;25:3560-70. DOI
57. Yao J, Ji P, Sheng N, et al. Hierarchical core-sheath polypyrrole@carbon nanotube/bacterial cellulose macrofibers with high electrochemical performance for all-solid-state supercapacitors. *Electrochim Acta* 2018;283:1578-88. DOI
58. Sheng N, Chen S, Yao J, et al. Polypyrrole@TEMPO-oxidized bacterial cellulose/reduced graphene oxide macrofibers for flexible all-solid-state supercapacitors. *Chem Eng J* 2019;368:1022-32. DOI
59. Guan F, Xie Y, Wu H, et al. Silver nanowire-bacterial cellulose composite fiber-based sensor for highly sensitive detection of pressure and proximity. *ACS Nano* 2020;14:15428-39. DOI PubMed

60. Zhou X, Liu Y, Du C, et al. Layer-by-layer engineered silicon-based sandwich nanomat as flexible anode for lithium-ion batteries. *ACS Appl Mater Interfaces* 2019;11:39970-8. DOI PubMed
61. Wu Y, Hu H, Yuan C, Song J, Wu M. Electrons/ions dual transport channels design: Concurrently tuning interlayer conductivity and space within re-stacked few-layered MXenes film electrodes for high-areal-capacitance stretchable micro-supercapacitor-arrays. *Nano Energy* 2020;74:104812. DOI
62. Hiraoki R, Ono Y, Saito T, Isogai A. Molecular mass and molecular-mass distribution of TEMPO-oxidized celluloses and TEMPO-oxidized cellulose nanofibrils. *Biomacromolecules* 2015;16:675-81. DOI PubMed
63. Zhou Y, Saito T, Bergström L, Isogai A. Acid-Free preparation of cellulose nanocrystals by TEMPO oxidation and subsequent cavitation. *Biomacromolecules* 2018;19:633-9. DOI PubMed
64. Iwamoto S, Kai W, Isogai A, Iwata T. Elastic modulus of single cellulose microfibrils from tunicate measured by atomic force microscopy. *Biomacromolecules* 2009;10:2571-6. DOI PubMed
65. Saito T, Kuramae R, Wohlert J, Berglund LA, Isogai A. An ultrastrong nanofibrillar biomaterial: the strength of single cellulose nanofibrils revealed via sonication-induced fragmentation. *Biomacromolecules* 2013;14:248-53. DOI PubMed
66. Wegst UG, Bai H, Saiz E, Tomsia AP, Ritchie RO. Bioinspired structural materials. *Nat Mater* 2015;14:23-36. DOI PubMed
67. Bush S, Torres F, Methven J. Rheological characterisation of discrete long glass fibre (LGF) reinforced thermoplastics. *Composites Part A* 2000;31:1421-31. DOI
68. Torres F, Bush S. Sheet extrusion and thermoforming of discrete long glass fibre reinforced polypropylene. *Composites Part A* 2000;31:1289-94. DOI
69. Ma C, Cao W, Zhang W, et al. Wearable, ultrathin and transparent bacterial celluloses/MXene film with Janus structure and excellent mechanical property for electromagnetic interference shielding. *Chem Eng J* 2021;403:126438. DOI
70. Shahzad F, Alhabeb M, Hatter CB, et al. Electromagnetic interference shielding with 2D transition metal carbides (MXenes). *Science* 2016;353:1137-40. DOI PubMed
71. Olsson RT, Azizi Samir MA, Salazar-Alvarez G, et al. Making flexible magnetic aerogels and stiff magnetic nanopaper using cellulose nanofibrils as templates. *Nat Nanotechnol* 2010;5:584-8. DOI PubMed
72. Sun Y, Quan Q, Meng H, et al. Enhanced neurite outgrowth on a multiblock conductive nerve scaffold with self-powered electrical stimulation. *Adv Healthc Mater* 2019;8:e1900127. DOI PubMed
73. Eskilson O, Lindström SB, Sepulveda B, et al. Self-assembly of mechanoplasmonic bacterial cellulose-metal nanoparticle composites. *Adv Funct Mater* 2020;30:2004766. DOI
74. Morales-Narváez E, Golmohammadi H, Naghdi T, et al. Nanopaper as an optical sensing platform. *ACS Nano* 2015;9:7296-305. DOI PubMed
75. Liu Y, Wang S, Wang Z, et al. The in situ synthesis of silver nanoclusters inside a bacterial cellulose hydrogel for antibacterial applications. *J Mater Chem B* 2020;8:4846-50. DOI PubMed
76. Wasim M, Mushtaq M, Khan SU, et al. Development of bacterial cellulose nanocomposites: an overview of the synthesis of bacterial cellulose nanocomposites with metallic and metallic-oxide nanoparticles by different methods and techniques for biomedical applications. *J Ind Text* 2020. DOI
77. Liu Y, Zhang Y, Zhang Y, et al. MoC nanoparticle-embedded carbon nanofiber aerogels as flow-through electrodes for highly efficient pseudocapacitive deionization. *J Mater Chem A* 2020;8:1443-50. DOI
78. Anton-Sales I, Roig-Sanchez S, Sánchez-Guisado MJ, Laromaine A, Roig A. Bacterial nanocellulose and titania hybrids: cytocompatible and cryopreservable cell carriers. *ACS Biomater Sci Eng* 2020;6:4893-902. DOI PubMed
79. Liu R, Ma L, Niu G, et al. Oxygen-deficient bismuth oxide/graphene of ultrahigh capacitance as advanced flexible anode for asymmetric supercapacitors. *Adv Funct Mater* 2017;27:1701635. DOI
80. Roig-sanchez S, Jungstedt E, Anton-sales I, et al. Nanocellulose films with multiple functional nanoparticles in confined spatial distribution. *Nanoscale Horiz* 2019;4:634-41. DOI
81. Jiang S, Hu Q, Xu M, et al. Crystalline CdS/MoS_2 shape-controlled by a bacterial cellulose scaffold for enhanced photocatalytic hydrogen evolution. *Carbohydr Polym* 2020;250:116909. DOI PubMed
82. Ferreira-Neto EP, Ullah S, da Silva TCA, et al. Bacterial nanocellulose/MoS_2 hybrid aerogels as bifunctional adsorbent/photocatalyst membranes for in-flow water decontamination. *ACS Appl Mater Interfaces* 2020;12:41627-43. DOI PubMed
83. Lai F, Miao YE, Huang Y, Zhang Y, Liu T. Nitrogen-doped carbon nanofiber/molybdenum disulfide nanocomposites derived from bacterial cellulose for high-efficiency electrocatalytic hydrogen evolution reaction. *ACS Appl Mater Interfaces* 2016;8:3558-66. DOI PubMed
84. Wang P, Geng Z, Gao J, et al. $Zn_xCd_{1-x}S$/bacterial cellulose bionanocomposite foams with hierarchical architecture and enhanced visible-light photocatalytic hydrogen production activity. *J Mater Chem A* 2015;3:1709-16. DOI
85. Fei Y, Liang M, Zhou T, Chen Y, Zou H. Unique carbon nanofiber@Co/C aerogel derived bacterial cellulose embedded zeolitic imidazolate frameworks for high-performance electromagnetic interference shielding. *Carbon* 2020;167:575-84. DOI
86. Cui J, Xu X, Yang L, et al. Soft foam-like UiO-66/polydopamine/bacterial cellulose composite for the removal of aspirin and tetracycline hydrochloride. *Chem Eng J* 2020;395:125174. DOI
87. Ma X, Lou Y, Chen X, Shi Z, Xu Y. Multifunctional flexible composite aerogels constructed through in-situ growth of metal-organic framework nanoparticles on bacterial cellulose. *Chem Eng J* 2019;356:227-35. DOI
88. Chen LF, Huang ZH, Liang HW, Guan QF, Yu SH. Bacterial-cellulose-derived carbon nanofiber@MnO_2 and nitrogen-doped carbon nanofiber electrode materials: an asymmetric supercapacitor with high energy and power density. *Adv Mater* 2013;25:4746-52. DOI PubMed

89. Gupta A, Briffa SM, Swingler S, et al. Synthesis of silver nanoparticles using curcumin-cyclodextrins loaded into bacterial cellulose-based hydrogels for wound dressing applications. *Biomacromolecules* 2020;21:1802-11. DOI PubMed PMC
90. Zrínyi M, Barsi L, Büki A. Ferrogel: a new magneto-controlled elastic medium. *Polym Gels and Netw* 1997;5:415-27. DOI
91. Bonini M, Lenz S, Giorgi R, Baglioni P. Nanomagnetic sponges for the cleaning of works of art. *Langmuir* 2007;23:8681-5. DOI PubMed
92. Liang H, Guan Q, Zhu Z, et al. Highly conductive and stretchable conductors fabricated from bacterial cellulose. *NPG Asia Mater* 2012;4:e19. DOI
93. Wu ZY, Li C, Liang HW, Chen JF, Yu SH. Ultralight, flexible, and fire-resistant carbon nanofiber aerogels from bacterial cellulose. *Angew Chem Int Ed Engl* 2013;52:2925-9. DOI PubMed
94. Elkhatat AM, Al-Muhtaseb SA. Advances in tailoring resorcinol-formaldehyde organic and carbon gels. *Adv Mater* 2011;23:2887-903. DOI PubMed
95. Yu W, Lin W, Shao X, Hu Z, Li R, Yuan D. High performance supercapacitor based on Ni_3S_2/carbon nanofibers and carbon nanofibers electrodes derived from bacterial cellulose. *J Power Sources* 2014;272:137-43. DOI
96. Xu Z, He M, Zhou Y, et al. Spider web-like carbonized bacterial cellulose/$MoSe_2$ nanocomposite with enhanced microwave attenuation performance and tunable absorption bands. *Nano Res* 2021;14:738-46. DOI
97. Zhou S, Qi H. A sustainable natural nanofibrous confinement strategy to obtain ultrafine Co_3O_4 nanocatalysts embedded in N-enriched carbon fibers for efficient biomass-derivative in situ hydrogenation. *Nanoscale* 2020;12:17373-84. DOI PubMed
98. Lai F, Yong D, Ning X, Pan B, Miao YE, Liu T. Bionanofiber assisted decoration of few-layered $MoSe_2$ nanosheets on 3D conductive networks for efficient hydrogen evolution. *Small* 2017;13:1602866. DOI PubMed
99. Lai F, Miao YE, Zuo L, Lu H, Huang Y, Liu T. Biomass-derived nitrogen-doped carbon nanofiber network: a facile template for decoration of ultrathin nickel-cobalt layered double hydroxide nanosheets as high-performance asymmetric supercapacitor electrode. *Small* 2016;12:3235-44. DOI PubMed
100. Huang Y, Lin Z, Zheng M, et al. Amorphous Fe_2O_3 nanoshells coated on carbonized bacterial cellulose nanofibers as a flexible anode for high-performance lithium ion batteries. *J Power Sources* 2016;307:649-56. DOI
101. Wang W, Sun Y, Liu B, Wang S, Cao M. Porous carbon nanofiber webs derived from bacterial cellulose as an anode for high performance lithium ion batteries. *Carbon* 2015;91:56-65. DOI
102. Paraknowitsch JP, Thomas A. Doping carbons beyond nitrogen: an overview of advanced heteroatom doped carbons with boron, sulphur and phosphorus for energy applications. *Energy Environ Sci* 2013;6:2839. DOI